Earth and Planetary Science Letters 408 (2014) 331–340

Contents lists available at ScienceDirect

Earth and Planetary Science Letters

www.elsevier.com/locate/epsl

Structure of the carbon isotope excursion in a high-resolution lacustrine Paleocene–Eocene Thermal Maximum record from central China

Zuoling Chen[a,b,*], Xu Wang[a], Jianfang Hu[c], Shiling Yang[a], Min Zhu[d], Xinxin Dong[a], Zihua Tang[a], Ping'an Peng[c], Zhongli Ding[a,*]

[a] *Key Laboratory of Cenozoic Geology and Environment, Institute of Geology and Geophysics, Chinese Academy of Sciences, Beijing 100029, China*
[b] *University of Chinese Academy of Sciences, Beijing 100049, China*
[c] *Guangzhou Institute of Geochemistry, Chinese Academy of Sciences, Guangzhou 510640, China*
[d] *Key Laboratory of Vertebrate Evolution and Human Origins, Institute of Vertebrate Paleontology and Paleoanthropology, Chinese Academy of Sciences, Beijing 100044, China*

ARTICLE INFO

Article history:
Received 24 February 2014
Received in revised form 5 October 2014
Accepted 19 October 2014
Available online 4 November 2014
Editor: J. Lynch-Stieglitz

Keywords:
PETM
carbon isotope excursion
positive feedback
lacustrine
Nanyang Basin

ABSTRACT

The carbon isotope excursion (CIE) associated with the Paleocene–Eocene Thermal Maximum (PETM) has been recognized for the first time in the micritic carbonate, total organic carbon (TOC) and black carbon (BC) contained within the lacustrine sediments from the Nanyang Basin, central China. The remarkably large excursion (∼ −6‰) in the $\delta^{13}C_{TOC}$ and $\delta^{13}C_{BC}$ values is possibly attributable to increased humidity and elevated pCO_2 concentration. The ∼ −4‰ CIE recorded in the $\delta^{13}C_{calcite}$, reflecting the average isotope change of the watershed system, is consistent with that observed in planktonic foraminifera. This correspondence suggests that the true magnitude of the carbon isotope excursion in the ocean–atmosphere system is likely close to −4‰. The ∼10 m excursion onset in our multi-proxy $\delta^{13}C$ records demonstrates that the large input of ^{13}C-depleted carbon into the ocean–atmosphere system was not geologically instantaneous. Despite difference and somewhat smoothness in detailed pattern of the CIE due to localized controls on different substrates, inorganic and organic $\delta^{13}C$ data generally depict a gradual excursion onset at least over timescales of thousands of years. In addition, continental temperature reconstruction, based on the distribution of membrane lipids of bacteria, suggests a warming of ∼4 °C prior to the PETM and ∼7 °C increase in temperature during the PETM. The temperature data are overall similar in pattern and trend to the $\delta^{13}C$ change across the PETM. These observations, combined with pre-CIE warming, are in line with the idea that ^{13}C-depleted carbon release operated as a positive feedback to temperature, suggesting supply from one or more large organic carbon reservoirs on Earth's surface.

1. Introduction

The Paleocene–Eocene Thermal Maximum (PETM; ∼55.5 Ma) is a geologically abrupt global warming event superimposed on a long-term warming trend of the early Cenozoic (Kennett and Stott, 1991; Zachos et al., 2001). The onset of the event occurred within ∼20 kyr and the complete event lasted ∼170 kyr (Röhl et al., 2007; Charles et al., 2011). During the PETM, temperatures increased abruptly by at least 5 °C globally (Kennett and Stott, 1991; Thomas et al., 1999; Zachos et al., 2003; Tripati and Elderfield, 2005) while stronger warming of up to 8 °C has been reported at middle and high latitudes (Sluijs et al., 2006; Zachos et al., 2006; Weijers et al., 2007a). The short-lived warming events induced severe environmental perturbation, including mass extinction of benthic foraminifera, rapid northward migration of plants in North America, and mammalian turnover (Thomas, 1998; Wing et al., 2005; Clyde and Gingerich, 1998).

Associated with the PETM are a globally recognized negative carbon isotope excursion (CIE) (Kennett and Stott, 1991; McInerney and Wing, 2011) and widespread dissolution of deep-sea carbonates (Zachos et al., 2005), which indicate more than 2000 gigatons of ^{13}C-depleted carbon entering the ocean–atmosphere system

---

* Corresponding authors at: Institute of Geology and Geophysics, CAS, 19 Beitucheng Western Road, Chaoyang District, Beijing 100029, China. Tel.: +86 10 8299 8378; fax: +86 10 6201 0846.

E-mail addresses: chenzl@mail.iggcas.ac.cn (Z. Chen), zlding@mail.iggcas.ac.cn (Z. Ding).

http://dx.doi.org/10.1016/j.epsl.2014.10.027

(Dickens et al., 1995; Zachos et al., 2005; Panchuk et al., 2008; Zeebe et al., 2009; Cui et al., 2011). This is comparable in magnitude to that which could occur over the coming centuries, and the PETM has thus become a focus for studies of past climate change. To date, however, there are still several first-order controversies concerning the carbon injection during the PETM. These include the source of carbon and its relationship to temperature. Possible sources of ^{13}C-depleted carbon include the injection of thermogenic methane (Svensen et al., 2004), impact of a comet (Kent et al., 2003), dissociation of seafloor methane hydrates (Dickens et al., 1995), combustion of the Paleocene peatlands (Kurtz et al., 2003), and permafrost thawing (DeConto et al., 2012). Underlying the current debate is whether the ^{13}C-depleted carbon release is a positive feedback to the temperature rise. The key to solve the debate is to clearly define the magnitude and shape of the CIE and its relationship to temperature.

Since the mixing time of carbon in the exogenic carbon reservoirs (including the atmosphere, terrestrial biosphere and ocean) is on the time-scale of $\sim 10^3$ yr (Kump and Arthur, 1999), in theory the general character of the CIE recorded in the continental and marine sediments should be identical and synchronous. There is, however, a significant discrepancy in the pattern and magnitude of the CIE in existing PETM records, depending on locations and analyzed substrates (Bains et al., 1999; Giusberti et al., 2007; McInerney and Wing, 2011; Sluijs and Dickens, 2012). For example, the general magnitude of the CIE from benthic foraminifera and bulk marine carbonate is 2 to 2.5‰ (Kennett and Stott, 1991; Bains et al., 1999; Thomas et al., 2002), and planktonic foraminiferal records shows up to 4‰ negative shift (Thomas et al., 2002; Zachos et al., 2006; Handley et al., 2008), while most terrestrial bulk organic and paleosol carbonates and biomarkers records yield excursion of ∼4–8‰ (Koch et al., 1992; Schmitz and Pujalte, 2003; Pagani et al., 2006a; Handley et al., 2008). Efforts to reconcile the ∼3‰ difference in terrestrial and marine records have focused on two hypotheses. The first hypothesis suggests that marine carbonates fail to record the full magnitude of the CIE, due to truncation caused by severe dissolution of carbonates or acidification (Zachos et al., 2005; Pagani et al., 2006a; McCarren et al., 2008), whilst the other hypothesis suggests that greater δ^{13}C discrimination due to increasing humid, or plant community change amplifies the terrestrial CIE (Bowen et al., 2004; Smith et al., 2007).

Another unsolved problem is the pattern of the CIE. Previous study, based on bulk carbonate records, showed that minimum δ^{13}C values were reached in a stepped manner, suggestive of a pulsed liberation of carbon (Bains et al., 1999). Recently, many high-resolution stratigraphic records have challenged this conclusion and indicated a single, instantaneous addition of ^{13}C-depleted carbon to the ocean–atmosphere system (Thomas et al., 2002; Giusberti et al., 2007). Even the greatly expanded sections from the New Jersey shelf areas did not see the feature of the stepped manner (Sluijs et al., 2007). So far, there are no any two records which share the consistent pattern of the CIE. Therefore, there is a critical need for further PETM records, especially high-resolution terrestrial carbon isotope records to tease out the pattern and magnitude of the CIE.

Here we recovered the first lacustrine PETM section based on high-resolution geochemical proxies from the Nanyang Basin, central China. Our new high-resolution terrestrial carbon isotope data provide a unique opportunity to define the structure of the CIE and its relationship to temperature in the terrestrial carbon reservoir.

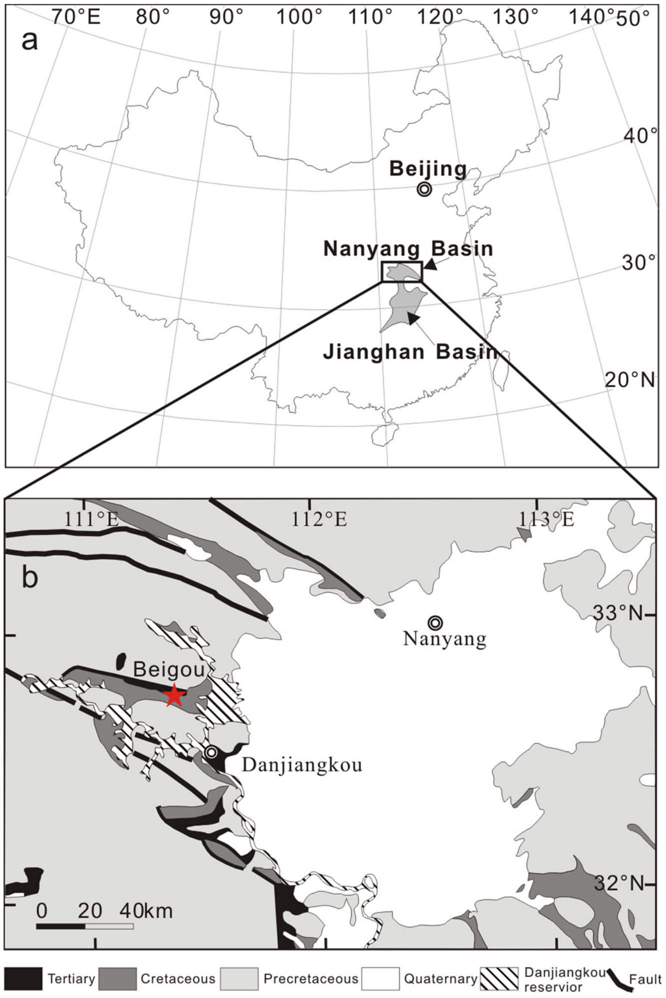

Fig. 1. Paleogeographic location (a) and geological sketch map (b) of the studied site. The red star indicates the study site. (For interpretation of the references to color in this figure legend, the reader is referred to the web version of this article.)

2. Material and methods

2.1. Geologic setting and sampling

The Nanyang Basin, located in the eastern Qinling Mountain region, is a large intermontane Mesozoic–Cenozoic down-faulted basin (Feng et al., 1997). During the late Mesozoic, the Yanshanian Movement brought about the uplift of pre-Cretaceous strata to the south and new differentiation of crustal activity, especially the compressive folding and faulting throughout the area. Specifically, the west part of the region uplifted, while the east part subsided. As a result, a large fault basin – Nanyang Basin – formed surrounding Nanyang during the late Cretaceous period, which received very thick deposits in the Cenozoic (Fig. 1).

At the Nanyang Basin, the late Cretaceous–early Eocene deposits are mostly developed with clear stratigraphic sequences, including the Hugang, Baiying and Yuhuangding formations (Feng et al., 1999). The Hugang Formation is predominately made up of fine clastics, indicating a shallow fluvio-lacustrine facies. The Baiying Formation consists of thick lacustrine marls with interbedded calcareous mudstones. The Yuhuangding Formation, characterized by grayish-pink marls with interbedded reddish siltstones and calcareous mudstones, is interpreted as representing deep lacustrine facies environments. These strata do not contain any significant unconformities and no evidence indicates any existence of hiatus.

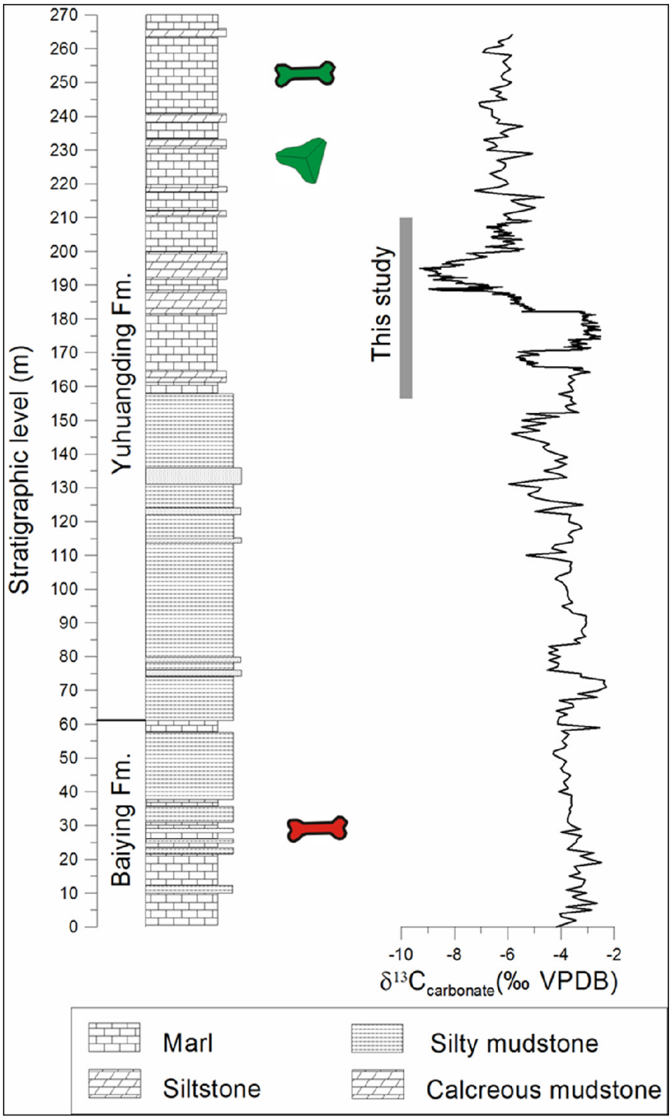

Fig. 2. Biostratigraphy (Ma and Cheng, 1991; Huang et al., 2004; Zhao and Guo, 1995) and chemostratigraphy (Zhu et al., 2010) of the studied area. Paleocene fossils are indicated with red symbols and early Eocene with green. (For interpretation of the references to color in this figure legend, the reader is referred to the web version of this article.)

Biostratigraphic investigations constrain the chronology of the deposits in this basin. A simplicidentate mammal, *Hanomys malcolmi* found in the Baiying Formation assigns this formation to the Paleocene (Huang et al., 2004), while the *Heptodon–Rhombomylus* Assemblage Zone found in the lower part of the Yuhuangding Formation indicates an early Eocene age (Fig. 2) (Ma and Cheng, 1991; Ting et al., 2003). Palynostratigraphy further defines the Paleocene/Eocene boundary in the lower part of the Yuhuangding Formation (Zhao and Guo, 1995). Our previous work has detected the CIE in the lower part of the Yuhuangding Formation based on a long-term micrite δ^{13}C record (Fig. 2) (Zhu et al., 2010). However, intrabasinal sedimentary variations in facies and lithology may complicate the record. For this study, we re-sampled a successive Paleocene/Eocene boundary stratigraphic section (Beigou: 32°43.9′N, 111°27.6′E) with relatively homogeneous facies close to the depocenter of the basin (Fig. 1). We mainly focused on the 50-m-thick deposits in the lower part of the Yuhuangding Formation (Fig. 2), and collected samples at a resolution of 2 to 20 cm.

2.2. Micritic carbonate δ^{13}C measurements

Samples of micritic carbonate (∼150 μg) were drilled from polished surface under a microscope using a dental drill. Sparry and pore-filling, diagenetic calcite phases were avoided during sampling. Samples were reacted with 100% orthophosphoric acid at 72 °C for 1 h using a GasBench II carbonate preparation device interfaced with a MAT253 isotope ratio mass spectrometer. Stable isotope results are reported relative to the Vienna PeeDee Belemnite (VPDB) standard with an external analytical precision of ±0.15‰.

2.3. Total organic carbon (TOC) and black carbon (BC) isotope ratios

For $\delta^{13}C_{TOC}$ analyses, samples were treated with 1 N HCl to remove carbonate, then rinsed with distilled water, and dried at 50 °C. For the $\delta^{13}C_{BC}$ measurements, the carbonates and part of the silicates in the samples were removed with 3 N HCl and HF/HCl (10 N:1 N) in sequence. The treated samples were then oxidized by a solution of $K_2Cr_2O_7/H_2SO_4$ (0.1 mol/L:2 mol/L) at 55 °C for 60 h to remove soluble organic matter and kerogen. After the treatment, the remaining refractory carbon is called BC. All δ^{13}C analyses were performed with a Flash 1112 elemental analyzer, connected to a Finnigan MAT253 isotope ratio mass spectrometer. Analytical precision is better than ±0.2‰. All values are reported relative to the VPDB standard.

2.4. Carbonate compositions and petrographic analysis

The mineralogical composition of 205 powered carbonate samples was determined by X-ray diffraction (XRD) using a Rigaku D/MAX 2400 diffractometer (Japan). An aliquot of the powdered sample was packed into an aluminum holder and scanned from 2° to 72° 2θ at 8° 2θ/min using Cu Kα radiation at 40 kV, 60 mA. The compositions of carbonate samples were also determined by standard XRD semiquantitative methods (Chung, 1974).

Polished thin sections were prepared for petrographic analysis from two typical micritic marls (pre-excursion and excursion samples) cut perpendicular to the horizontal plane of sedimentary bedding. The selected samples were also studied for crystal size and morphology using a LEO1450VP scanning electron microscope (SEM) (Fig. 3).

2.5. Glycerol dialkyl glycerol tetraether (GDGT) analyses

Organic compounds were extracted from powered and freeze-dried sediment samples by Soxhlet extractor with dichloromethane (DCM)/methanol (MeOH) (2:1; v/v) for 72 h. The excess solvent was removed using rotary evaporation under vacuum and the extracts were separated into apolar and polar fractions by an activated Al_2O_3 column chromatography with hexane/DCM (9:1; v/v) and DCM/MeOH (1:1; v/v) as sequential eluents, respectively. The polar fractions, containing the branched GDGTs, were concentrated by rotary evaporation, re-dissolved in a hexane/isopropanol (99:1; v/v) mixture, and then passed through a 0.45 μm PTFE filter. Subsequently, the filtrates were analyzed for branched GDGTs by high performance liquid chromatography/atmospheric pressure chemical ionization-mass spectrometry (HPLC/APCI-MS). The detailed HPLC/APCI-MS instrument methods were performed following Zhou et al. (2011) using an Agilent 1200 series liquid chromatograph equipped with an auto-injector and ChemStation chromatography management software. The cyclization ratio of branched tetraethers (CBT) and the methylation index of branched tetraethers (MBT) are defined as (Weijers et al., 2007b):

$$\mathrm{CBT} = -\log\left(\frac{[\mathrm{Ib}+\mathrm{IIb}]}{[\mathrm{I}+\mathrm{II}]}\right) \tag{1}$$

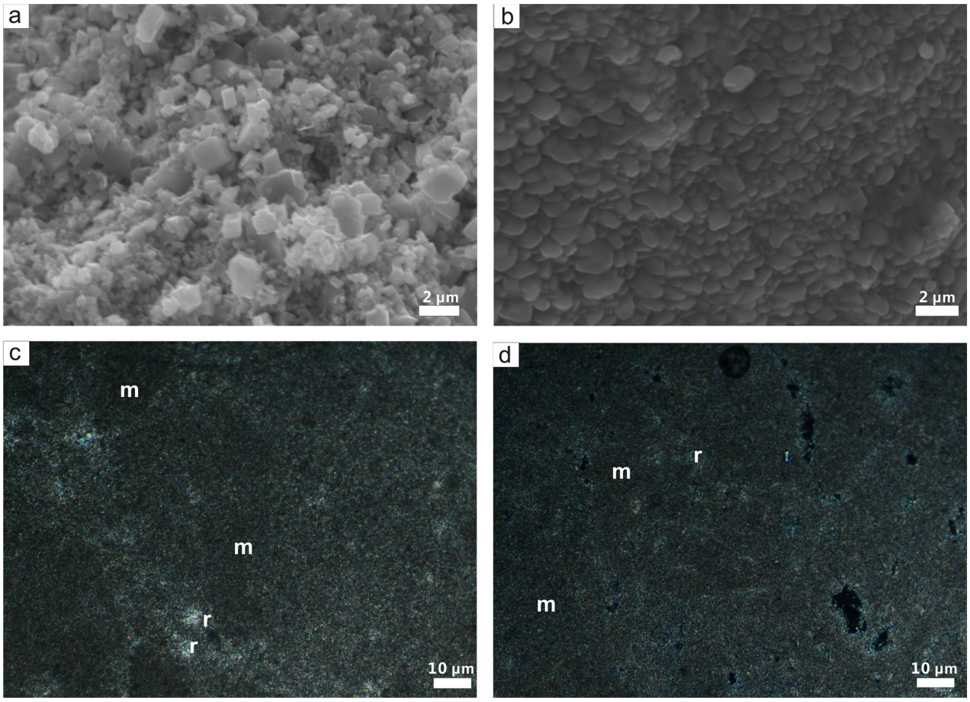

Fig. 3. Scanning electron microscope (SEM) images of the pre-excursion sample (a) and the excursion sample (b), and photomicrographs from thin sections of the pre-excursion sample (c) and the excursion sample (d) showing little fine-grained recrystallization (r) of primary micrite (m).

$$\mathrm{MBT} = \frac{[\mathrm{I}+\mathrm{Ib}+\mathrm{Ic}]}{[\mathrm{I}+\mathrm{Ib}+\mathrm{Ic}]+[\mathrm{II}+\mathrm{IIb}+\mathrm{IIc}]+[\mathrm{III}+\mathrm{IIIb}+\mathrm{IIIc}]} \qquad (2)$$

Roman numbers correspond to different branched GDGTs: GDGTs I, II and III contain none, one or two extra methyl branches and can contain either one (Ib; IIb; IIIb) or two (Ic; IIc, IIIc) cyclopentyl moieties (Weijers et al., 2007b). Annual mean air temperature (MAT) was then calculated from the CBT and MBT using the calibration equation developed by Sun et al. (2011) based on Asian modern lake surface sediments:

$$\mathrm{MAT} = 6.803 - 7.062 \times \mathrm{CBT} + 37.090 \times \mathrm{MBT} \qquad (3)$$

3. Results

3.1. *Composition of carbonate minerals*

X-ray diffraction shows that mineral composition at the Beigou section is very simple, mainly including calcite, dolomite and quartz (Fig. 4), hence relative percentages of carbonate minerals are estimated from the bulk mineral diffractograms using the intensity of the strongest peak for each mineral (Chung, 1974). Prior to the CIE, there is abundant dolomite (28 to 100%) with a variable content of calcite in primary carbonate (Table S1). From the onset of the CIE, however, dolomite disappears and calcite is the only carbonate precipitate mineral (Fig. 5).

3.2. *Nanyang micritic carbonate, total organic carbon and black carbon $\delta^{13}C$ records*

Micritic $\delta^{13}C_{\mathrm{carbonate}}$ values range between −9.3‰ and −2.6‰ with an average of −5.4‰ over the whole section (Table S1). Subtle fluctuations around −3.7‰ in $\delta^{13}C_{\mathrm{carbonate}}$ values are observed between 0 and 20 m (Fig. 5). Above this, the $\delta^{13}C_{\mathrm{carbonate}}$ values drop slowly and gradually to the minimum (−9.3‰) from 20 m to 33 m, with a sharp spike of −1.3‰ for 1 m (37.1–38.1 m). Following this negative shift, the $\delta^{13}C_{\mathrm{carbonate}}$ values increase slowly and finally stabilize around −6‰ at 40 m and for the remainder of the section. The recovery values of $\delta^{13}C_{\mathrm{carbonate}}$ are ~2‰ more negative than the pre-excursion values.

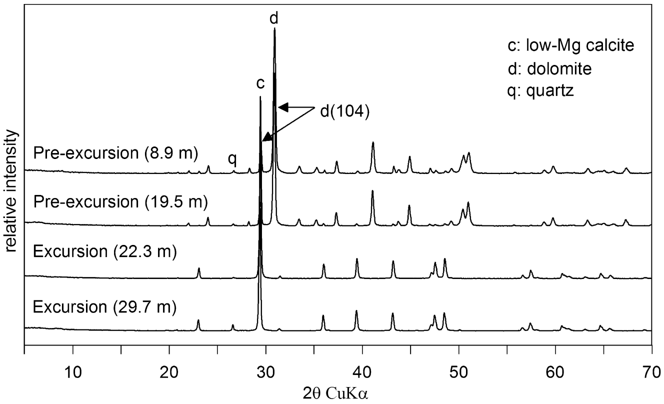

Fig. 4. XRD patterns of representative samples, including pre-excursion samples and excursion samples.

$\delta^{13}C_{\mathrm{TOC}}$ and $\delta^{13}C_{\mathrm{BC}}$ values at the Beigou section broadly show similar change. Both of them range between −28.6‰ and −20‰ with an average value of −24‰ (Table S2). These are typical values for C_3 plants (i.e. values range between −34‰ and −20‰). $\delta^{13}C_{\mathrm{TOC}}$ and $\delta^{13}C_{\mathrm{BC}}$ values fluctuate around a relatively stable background level (−22‰) between 0 and 20 m (Fig. 5). As with the $\delta^{13}C_{\mathrm{carbonate}}$ record, the $\delta^{13}C_{\mathrm{TOC}}$ and $\delta^{13}C_{\mathrm{BC}}$ values decrease gradually from 20 m, but punctuated by 2.3‰ and 3.4‰ transient positive shifts around 24 m respectively, and then progress to the minimum (~ −28‰) at 30 m. Above this, the values increase slowly and finally stabilize around −24‰ at 40 m and for the remainder of the section.

3.3. *Paleocene–Eocene continental temperature estimates*

The BIT values, a proxy for the relative amount of soil-derived branched GDGTs versus aquatic archaeal GDGTs (Hopmans et al., 2004), range from 0.31 to 0.98 (Table S3), suggesting considerable

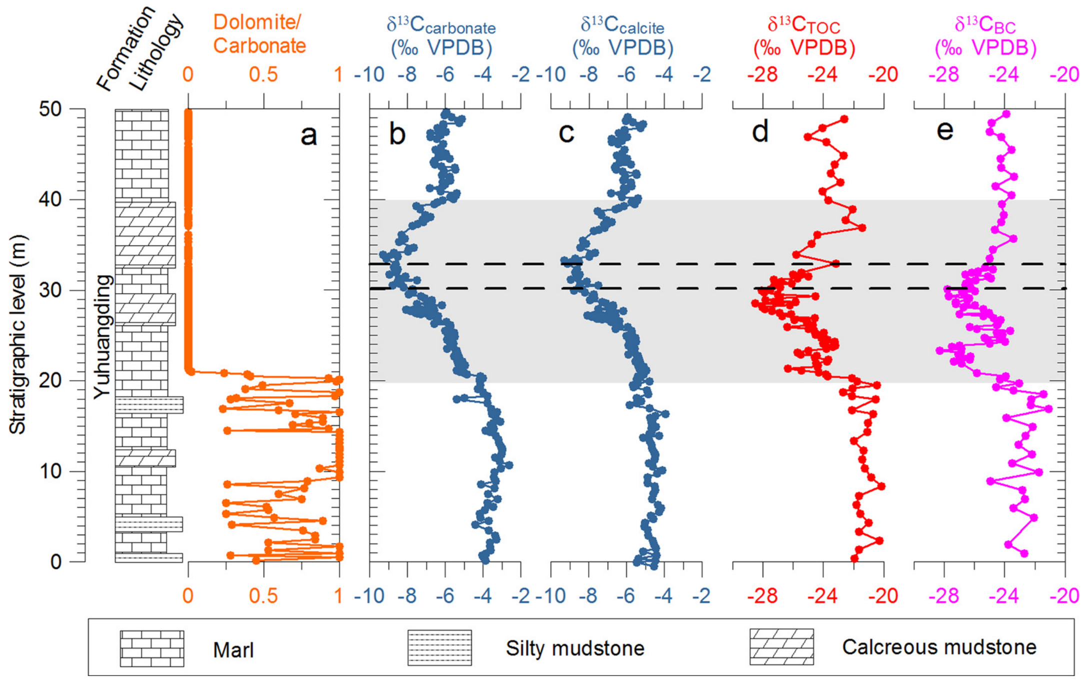

Fig. 5. Mineral composition of carbonate (a), and stable carbon isotope ratios of micritic carbonate (b), calcite (c), total organic carbon (d) and black carbon (e). $\delta^{13}C_{calcite}$ values are determined by correcting $\delta^{13}C_{carbonate}$ using the mineral composition of carbonate. The shaded area highlights the PETM CIE. The dashed lines show a delay of $\delta^{13}C_{calcite}$ record.

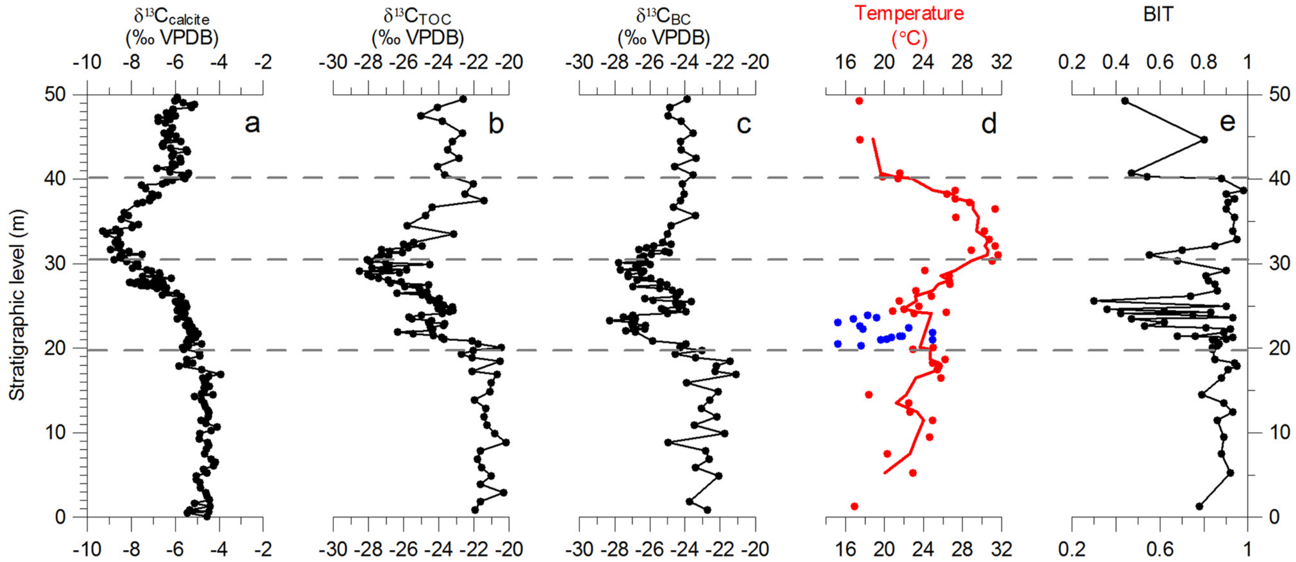

Fig. 6. Carbon isotope, BIT index, and temperature records from the Beigou section. Calcite $\delta^{13}C$ values (a). Total organic carbon $\delta^{13}C$ values (b). Black carbon $\delta^{13}C$ values (c). Temperature estimates from MBT and CBT (d). BIT index (e). The red solid line shows the three-points running average of red dots. The blue dots are temperature anomalies which might be an artifact caused by low GDGTs fraction with carbonate content as high as 99%. Gray dashed lines represent the onset, the maximum and the end of the PETM, respectively. (For interpretation of the references to color in this figure legend, the reader is referred to the web version of this article.)

input of soil-derived GDGTs. The MBT/CBT paleothermometry data show that a gradual increase in temperature from 20 to 24 °C toward the onset of the CIE (Fig. 6), followed by a cooling trend around 22 m (blue dots in Fig. 6d), which might be an artifact caused by low GDGTs fraction with carbonate content as high as 99%. During the body of the CIE, temperatures increase gradually to 31 °C from 22 m to 31 m, and then slowly drop again to the initial values for the reminder of the section. Higher temperatures occur at the time of lighter $\delta^{13}C$ values (Fig. 6).

4. Discussion

4.1. Diagenetic and detrital effects on $\delta^{13}C_{carbonate}$

Dissolution/recrystallization processes during diagenesis of carbonate minerals can significantly alter the carbon isotope signal of authigenic carbonate (e.g., Garzione et al., 2004). SEM analyses show that the carbonate crystals are generally less than 2 μm in size (Figs. 3a and 3b). It has been suggested that fine- to very-fine grained carbonates are less susceptible to remineralization by diagenetic fluids because of their extremely low permeability

(Dickson and Coleman, 1980; Poulson and John, 2003). On the other hand, thin section analyses of two typical samples reveal that these carbonates are texturally wackestones with homogeneous micritic matrix (Figs. 3c and 3d), while microsparry calcite is rare and sparry calcite is absent, indicating that the original sedimentary fabric was not replaced after deposition. Overall, these petrographic features suggest that carbonates at the Beigou section have undergone little diagenetic alteration.

Detrital carbonate can also bias the isotopic composition of the carbonate that formed in situ (Leng et al., 2010). However, two lines of evidence suggest that allogenic carbonate did not significantly contribute to the isotopic composition of analyzed carbonates. Firstly, SEM analyses show that the pre-excursion sample predominantly of ∼1 μm-sized euhedral crystals of dolomite (Fig. 3a) and the excursion sample is composed of ∼2 μm-sized anhedral crystals of calcite (Fig. 3b). Their morphology is consistent with authigenic carbonate precipitated in the water column. The angular nature of the grains indicates that crystals had undergone little or no transportation or reworking. Secondly, thin sections analyses show no evidence for the existence of detrital grains (Figs. 3c and 3d). In summary, petrographic and mineralogical features, such as the homogeneous compositional and textural character of the carbonates, the absence of replacement textures support a direct primary origin and little or no diagenetic alteration for the carbonates. We thus conclude that the micritic $\delta^{13}C_{carbonate}$ values in this study could track the isotopic signal of dissolved inorganic carbon in lake water.

4.2. Bio- and chemostratigraphic recognition of the PETM

The Beigou section is predominately marl of lacustrine facies with very high abundance of carbonate, which induces too weak a magnetic signal to construct an age framework using paleomagnetic techniques. Therefore, we use biostratigraphic dating and carbon isotope stratigraphy to confine the PETM at the site.

Detailed mammal and pollen fossils investigations have constrained the Paleocene/Eocene boundary within the lower part of the Yuhuangding formation (Fig. 2) (Ma and Cheng, 1991; Zhao and Guo, 1995; Ting et al., 2003; Huang et al., 2004). Here our multiple $\delta^{13}C$ data show that carbon isotope values fluctuate around a relatively stable background level between 0 and 20 m ($\delta^{13}C_{carbonate}$: $\sim -3.7‰$; $\delta^{13}C_{TOC}$: $\sim -22‰$; $\delta^{13}C_{BC}$: $\sim -22‰$), and then shift gradually to the minimum around 31 m ($\delta^{13}C_{carbonate}$: $\sim -9.3‰$; $\delta^{13}C_{TOC}$: $\sim -28‰$; $\delta^{13}C_{BC}$: $\sim -28‰$), followed by a slow return to values slightly lower than the pre-excursion level (Fig. 5). These results definitely exhibit a general excursion pattern that is similar to that defined by marine and other terrestrial records (Kennett and Stott, 1991; Koch et al., 1992; Magioncalda et al., 2004; Bowen, 2013). Although the $\delta^{13}C$ values of each substrate could be affected by different factors at the Beigou section, terrestrial plants (black carbon), aquatic plants (total organic carbon) and lacustrine carbonate systems all document a large-magnitude carbon isotope excursion, demonstrating that a systematic negative carbon isotope shift occurred in the exogenic carbon reservoirs. The pronounced CIE recorded in the inorganic and organic substrates from 20 to 40 m, combined with biostratigraphy, confirms that the section spans the Paleocene/Eocene boundary and the PETM. We have thus established the first complete lacustrine record of the PETM, which is not associated with any formation boundary or major lithological change (Fig. 5).

The 20-m-thick CIE interval is greatly expanded relative to that found in existing deep-sea sections. High-resolution chronologies have been developed for terrestrial and marine sections and suggest a total PETM duration of 120–200 kyr (Norris and Röhl, 1999; Röhl et al., 2007; Aziz et al., 2008). If we assume a constant sedimentation rate for the Beigou section, our record yields a mean sedimentation rate of 10–16.7 cm/kyr across the PETM, which is almost ten times more rapid than that for most deep-sea sections. Therefore, our data might present a more detailed record of the CIE. Viewed together, multi-proxy $\delta^{13}C$ data clearly display two distinctive features: (1) that the carbon isotope values of three substrates show an excursion of $\sim -6‰$, which is substantially larger than that generally recorded in bulk marine carbonate and benthic foraminifera (McInerney and Wing, 2011); and (2) that all $\delta^{13}C$ curves generally show a gradual negative shift with transitional values, followed by an exponential return to initial values.

4.3. Magnitude of CIE

The magnitude of the CIE is critical for estimating the amounts of carbon addition during the PETM (Dickens et al., 1995) and evaluating the sensitivity of the climate system to the associated greenhouse gas forcing (Pagani et al., 2006b). Despite an abundance of carbon isotope records, some uncertainty still surrounds the full magnitude of the CIE, which shows a large variation between $-2‰$ and $-7‰$, depending on locations and analyzed substrates (McInerney and Wing, 2011; Sluijs and Dickens, 2012). The $\delta^{13}C$ values of black carbon could elucidate the isotopic composition in vegetation that was burnt, because it is inert and produced by the incomplete combustion of biomass (Schmidt and Noack, 2000). The $\delta^{13}C_{BC}$ values here show a prominent $\sim 6‰$ negative shift across the PETM which reflects the $\delta^{13}C$ signal of vegetation surrounding the lake (Fig. 5). The $\delta^{13}C_{BC}$ pattern is generally reproduced in the carbon isotope record of total organic carbon, a mixed contribution of aquatic and terrestrial plants (Fig. 5). This coincidence, both in trend and isotopic shift, suggests that the TOC was substantially influenced by terrestrial components and lake biological productivity might be low at that time. This explanation is indeed consistent with the BIT values (Fig. 6e), which also suggest significant contribution of terrestrial soil organic material (Hopmans et al., 2004). Importantly, the CIE from the total organic carbon and black carbon (approximately $-6‰$) is substantially larger than the CIE anomaly (about $-2.5‰$) generally recoded in bulk marine carbonate and benthic foraminifera (Thomas et al., 2002; Zachos et al., 2005).

Three potential scenarios have been proposed to explain the anomalous large CIE recorded in terrestrial organic substrates. Firstly, C_3 angiosperms are typically 3‰ depleted in ^{13}C in comparison with gymnosperms (Schouten et al., 2007), an effect likely related to the efficacy of water use (Chikaraishi and Naraoka, 2003). Thus, a notable increase of angiosperm flora relative to gymnosperms has been invoked to explain the large CIE as recorded by organic substrates (Smith et al., 2007; Schouten et al., 2007). To reconcile the difference of $\sim 3‰$ would require almost a 100% shift from gymnosperm to angiosperm vegetation across the PETM. However, this is inconsistent with palynological data which show that angiosperm taxa are the dominant palynomorph and no noticeable change in the taxonomic composition occurs in the Yuhuangding Formation (Zhao and Guo, 1995). Secondly, increased ambient air humidity can lead to an increase in stomatal conductance and in turn amplify the carbon isotope fractionation associated with photosynthesis (Gröcke, 1998). It has thus been suggested that a 20% increase in soil moisture and humidity would result in a 1.5–2.1‰ amplification of the CIE in terrestrial substrates during the PETM (Bowen et al., 2004). In support of this explanation are the remarkable variations in primary carbonate at the Beigou section. Before the onset of the CIE, dolomite is the dominating carbonate precipitate mineral whereas it disappears and gives way to calcite during the PETM (Fig. 5). Often authigenic dolomite precipitates from a lake system are associated with highly evaporated lake water, suggestive of arid environment (Müller et al., 1972; Last, 1990). The sudden disappearance of primary dolomite in the strata is thus indicative of a transition from dry to wet across the PETM at the Nanyang Basin. These results are in line with the previous studies which indicate more precipitation at mid to high latitudes inferred from increased kaolinite deposits (Robert and Kennett, 1994; Bolle and Adatte, 2001) and *n*-alkane compound-specific hydrogen isotopic changes (Pagani et al., 2006a). Finally, the larger shift measured in terrestrial organic substrates could record a response to elevated CO_2 levels. Previous experiments have shown an increase in carbon isotope fractionation by land plants in response to increasing atmospheric pCO_2 concentration (Feng and Epstein, 1995). During the PETM, a massive input of ^{13}C-depleted carbon to the exogenic carbon reservoirs would necessitate a rise in atmospheric pCO_2, which in turn could amplify the $\delta^{13}C$ signal by ∼1–2‰ through increasing photosynthesis fractionation (Schubert and Hope Jahren, 2013). In summary, the larger excursion observed in the $\delta^{13}C_{BC}$ and $\delta^{13}C_{TOC}$ could bias the true magnitude of the CIE due to severe environmental disturbance during the PETM.

Further insight into the magnitude of the CIE is provided by the $\delta^{13}C$ values of micritic carbonate, with an excursion of ~ -5.5‰. Considering the fractionation differences between dolomite and calcite and assuming that both precipitated in isotopic equilibrium with lake water, we applied the method developed by Bristow et al. (2012) to correct the $\delta^{13}C_{carbonate}$ values of mixed carbonate minerals to that of calcite ($\delta^{13}C_{calcite}$) (Table S1), which track the carbon isotopic composition of the dissolved inorganic carbon (DIC) in the water mass. The resulting magnitude of the CIE is ~ -4‰ (Fig. 5). It is smaller than that recorded in organic substrates, but consistent with that observed in planktonic foraminifera (Thomas et al., 2002; Zachos et al., 2003; Handley et al., 2008; John et al., 2008). Clear interpretation of the carbon isotope ratios of authigenic carbonate is difficult because many factors contribute to the final isotopic composition of precipitated carbonates in lakes. In general, the carbon-isotope inventory in lake is controlled by three predominant factors: (1) the isotopic composition of inflowing waters; (2) CO_2 exchange between lake water and the atmosphere; (3) the balance between primary productivity and respiration of aquatic plants within the lake (Leng and Marshall, 2004). The highly alkaline lakes revealed by thick marl deposits, however, are less susceptible to biotic impacts, as the reservoir of dissolved inorganic carbon is so large. Generally, isotopically light CO_2 liberated by decay of terrestrial organic matter in the soil enters the soil waters and shallow groundwaters (Leng and Marshall, 2004), and ultimately inputs the lake system through runoff and rivers. Therefore, the $\delta^{13}C_{calcite}$ values should reflect the average isotope composition of DIC in the watershed system with varying degrees of equilibrium of the DIC with atmospheric CO_2 (Bade et al., 2004). Since all of the processes interact directly or indirectly with the atmospheric CO_2, the $\delta^{13}C_{calcite}$ values in this study might preserve time-averaged isotopic signal of atmospheric CO_2 and the CIE of ~ -4‰ is thus likely close to the true magnitude of carbon isotope anomaly in the exogenic carbon reservoirs. This result is consistent with others recently published (Cui et al., 2011; Sluijs and Dickens, 2012; Schoon et al., 2013), suggesting that the magnitude of the CIE in the ocean–atmosphere system may have been larger than −3 to −2.5‰ that has generally been accepted.

4.4. The shape of the CIE and its relationship to temperature

The details of the CIE have important implications for the triggering of the isotopically light carbon addition and the nature of potential feedbacks during the PETM (Stoll, 2005). Multisubstrate data from the Nanyang Basin clearly show distinct stratigraphic pattern of $\delta^{13}C$ change in the inorganic ($\delta^{13}C_{calcite}$) and organic fractions ($\delta^{13}C_{BC}$ and $\delta^{13}C_{TOC}$) across the PETM, with changes in the $\delta^{13}C_{calcite}$ being generally smoother than and lagging those in organic fractions (Fig. 5). Often carbonates spend millennia in Earth surface systems before they are deposited in the sedimentary record (Blair and Kalff, 1995; Tenzer et al., 1997). Hence, it is expected that the isotopic composition of authigenic carbonate should track time-averaged signal of dissolved inorganic carbon in the watershed systems around the lake. The mixing of carbon from isotopically distinct sources could result in the smoothed record and somewhat later onset and apparently a lagging arrival of the minimum values in $\delta^{13}C_{calcite}$.

In contrast, $\delta^{13}C_{BC}$ and $\delta^{13}C_{TOC}$ values show a relatively abrupt drop at the onset of the event, punctuated by a substantial increase in values around 24 m, and then gradually progress to the minimum values. Plants assimilate CO_2 directly from the atmosphere through photosynthesis and therefore could provide the most reliable record of the pattern of the CIE. The strong similarities between $\delta^{13}C_{BC}$ and $\delta^{13}C_{TOC}$ values, both in trend and isotopic shift, imply that the gradual carbon isotope excursion could unravel the true shape and profile of the CIE. These records are broadly similar in pattern to the majority of other well-resolved records worldwide (Bowen, 2013) except for a little more protracted excursion onset and a sharp positive shift during the progress of negative excursion. One possible explanation for the prolonged onset might be attributable to extremely high sedimentation rates of carbonate during the CIE onset, although there is no direct evidence for this due to a lack of robust age control. On the other hand, homogeneous marl depositions across the excursion onset demonstrate that changes in sedimentation rates are inapparent and could not significantly alter the pattern of the CIE onset. The sharp premature recovery to less negative $\delta^{13}C$ values in our organic substrates is also observed in some of the terrestrial records from Bighorn Basin (Baczynski et al., 2013; Bataille et al., 2013). It has been indicated that intensive runoff could significantly enhance erosion of "old" carbon in soils or ancient rocks, and as a result lead to anomalous change in organic $\delta^{13}C$ values (Clark et al., 2013). Accordingly, we interpret the sharp positive shift around 24 m as a mixture of autochthonous carbon ($\delta^{13}C$: ∼27‰) fixed during the PETM and allochthonous carbon ($\delta^{13}C$: ∼22‰) eroded from pre-PETM soils or rocks as recently suggested by Bataille et al. (2013) and Schneider-Mor and Bowen (2013). Changes in authigenic carbonates support this argument and imply enhanced hydrological cycle during the PETM.

Despite subtle differences and complexity of their explanations in the CIE for each substrate as discussed in above paragraphs, our high-resolution $\delta^{13}C$ curves generally depict a gradual excursion onset. The $\delta^{13}C$ values of each fraction could be controlled by different environmental variables, but all of them were directly or indirectly affected by atmospheric carbon pool. Taking account of the excessive excursion onset (∼10 m) in our records, we thus conclude that the carbon isotope excursion of atmospheric carbon reservoir possibly occurred in a gradual $\delta^{13}C$ decrease at least over timescales of thousands of years. Recently, Wright and Schaller (2013) examined records from apparently rhythmically layered shelf sediments to argue that the onset of the CIE occurred within 13 yr, and further suggested an instantaneous release of ^{13}C-depleted carbon. In contrast, the excursion onset was gradually completed within ∼10 m stratigraphic space in our records. It is highly inconceivable that ∼10-m-thick carbonates deposited in 13 yr, thus implying that their explanation is not feasible. Interestingly, our MBT/CBT paleothermometry data show a gradual increase of ∼7 °C and then a return to initial temperatures during the PETM, which is broadly similar in shape and trend to the carbon isotope records (Fig. 6). Specifically, while $\delta^{13}C$ values begin gradually to decrease at ∼20 m, the temperature starts to increase slowly. At approximately 31 m, the $\delta^{13}C$ ratios reach their minimum, and the temperature increases to its maximum; then, as the

$\delta^{13}C$ values increase, the temperature gradually returns to the initial values.

How a massive amount of ^{13}C-depleted carbon was injected remains the focus of much debate (Bains et al., 1999; Giusberti et al., 2007; Cui et al., 2011; Wright and Schaller, 2013). It has been suggested that greenhouse feedback might have played a pivotal role (Zachos et al., 2008), but no direct geological evidence exists. Here our high-resolution lacustrine records show that the minimum $\delta^{13}C$ values were reached in a gradual manner with some transitional values. Similarly, high-resolution $\delta^{13}C_{TOC}$ data from Spitsbergen also generally depict the same feature of the CIE as that revealed by our records (Cui et al., 2011). Taken together, $\delta^{13}C$ data of different substrates from different sites all present a gradual excursion onset, implying an enormous input of ^{13}C-depleted carbon into the atmosphere and ocean in a gradual manner rather than an instantaneous (Thomas et al., 2002; Giusberti et al., 2007) or pulsed manner (Bains et al., 1999) generally defined in marine sediments. Furthermore, the pattern and trend of the CIE from our records are mirrored in the temperature data (Fig. 6). This correspondence strongly demonstrates that the injection of ^{13}C-depleted carbon was intimately coupled with the temperature increase across the PETM. Taken with the fact of pre-CIE warming (Sluijs et al., 2007; Secord et al., 2010, this study), our observations provide a fundamental constraint on the event, in the form of a massive release of ^{13}C-depleted carbon that operated as a positive feedback to global warming. In particular, peak temperatures of sufficiently short duration are associated with the minimum carbon isotope values, implying that the carbon source was probably exhausted and the positive feedback ceased.

4.5. Implications for the carbon sources

Our high-resolution records clearly deconvolve the coupling of continental temperature change and the CIE. These findings have two important implications for the carbon sources. Firstly, the ∼4 °C warming occurred before the onset of the CIE does not correspond to any marked variation in multiple $\delta^{13}C$ data, indicating that the pre-CIE warming, if forced by increasing pCO_2, was likely attributable to volcano degassing with a $\delta^{13}C$ value identical to atmospheric CO_2 (Wieczorek et al., 2013). Secondly, the fact of pre-CIE warming (Sluijs et al., 2007; Secord et al., 2010, this study), coupled with evidence of covariance between temperature and $\delta^{13}C$ values during the CIE, is consistent with the idea that ^{13}C-depleted carbon release operated as a positive feedback to temperature rise, suggestive of carbon supply from one or more large organic carbon reservoirs on Earth's surface. Potentially, the combustion of the Paleocene peatlands might be responsible for the CIE (Kurtz et al., 2003). However, the $\delta^{13}C$ data of black carbon exhibit a similar CIE recorded in total organic carbon, indicating that this material was sourced from contemporaneous biomass rather than geologically old carbon. This is inconsistent with the prediction of wildfire hypothesis (Kurtz et al., 2003). Two other compelling possibilities for organic carbon feedback are permafrost (DeConto et al., 2012) and methane hydrates (Dickens et al., 1995). Because methane hydrate and permafrost reservoirs are relatively large and sensitive to temperature (Dickens et al., 1995; DeConto et al., 2012), our data are more consistent with the suggestion that most of ^{13}C-depleted carbon should be sourced from the decomposition of one or both of these organic carbon pools.

5. Conclusions

We have recovered the first high-resolution lacustrine PETM section from central China based on carbon isotope records of inorganic and organic fractions. Total organic carbon and black carbon record a 6‰ negative carbon isotope shift, while the $\delta^{13}C_{calcite}$ data reveal a carbon excursion of ∼ −4‰. Elevated pCO_2 concentration and enhanced precipitation, reflected by prominent changes in authigenic carbonate minerals, could be responsible for this remarkable large excursion. The CIE of ∼ −4‰ recorded in lacustrine calcite reflects the average isotopic anomaly in the watershed, which is consistent with that found in planktonic foraminifera (Thomas et al., 2002; Zachos et al., 2003). We thus suggest that the CIE of ∼ −4‰ observed in these subsystems may indeed reflect the true shift in the exogenic carbon reservoirs.

Multiple $\delta^{13}C$ data reveal a ∼10 m excursion onset, meaning that the PETM is very unlikely to be a single, decadal-scale carbon release event as suggested by Wright and Schaller (2013). Local factors, such as enhanced erosion of "old" carbon due to intensive runoff during the PETM, might complicate the isotopic signal of each substrate and lead to subtle difference or somewhat smoothness in the detailed pattern of the CIE, but inorganic and organic substrates broadly record a gradual CIE onset. This result, combined with the excessive excursion onset (∼10 m), probably indicates an enormous input of ^{13}C-depleted carbon into the ocean–atmosphere system in a gradual manner at least over timescales of thousands of years. Furthermore, the shape and trend of the CIE at the Nanyang Basin are generally mirrored in MBT/CBT paleothermometry data. These observations, in conjunction with pre-CIE warming, demonstrates that ^{13}C-depleted carbon release operated as a positive feedback to temperature rise, suggesting most of carbon supply from the decomposition of one or both of methane hydrates and permafrost.

Acknowledgements

We thank G.R. Dickens for a constructive comment that improved the manuscript; P.D. White for a review of the initial manuscript; S. Feng and H. Jiang for the field work; and L. Cui for experiments. We also thank F. McInerney and the other anonymous reviewer for their helpful comments, many of which have improved the final paper. This work was supported by the National Natural Science Foundation of China (grant 40730208), the (973) National Basic Research Program of China (grants 2012CB821905 and 2013CB956404), and the Strategic Priority Research Program of CAS (grant XDB03020503).

Appendix A. Supplementary material

Supplementary material related to this article can be found online at http://dx.doi.org/10.1016/j.epsl.2014.10.027.

References

Aziz, H.A., Hilgen, F.J., van Luijk, G.M., Sluijs, A., Kraus, M.J., Pares, J.M., Gingerich, P.D., 2008. Astronomical climate control on paleosol stacking patterns in the upper Paleocene–lower Eocene Willwood Formation, Bighorn Basin, Wyoming. Geology 36, 531–534.

Baczynski, A.A., McInerney, F.A., Wing, S.L., Kraus, M.J., Bloch, J.I., Boyer, D.M., Secord, R., Morse, P.E., Fricke, H.C., 2013. Chemostratigraphic implications of spatial variation in the Paleocene–Eocene Thermal Maximum carbon isotope excursion, SE Bighorn Basin, Wyoming. Geochem. Geophys. Geosyst. 14, 4133–4152.

Bade, D.L., Carpenter, S.R., Cole, J.J., Hanson, P.C., Hesslein, R.H., 2004. Controls of $\delta^{13}C$–DIC in lakes: geochemistry, lake metabolism, and morphometry. Limnol. Oceanogr. 49, 1160–1172.

Bains, S., Corfield, R.M., Norris, R.D., 1999. Mechanisms of climate warming at the end of the Paleocene. Science 285, 724–727.

Bataille, C.P., Mastalerz, M., Tipple, B.J., Bowen, G.J., 2013. Influence of provenance and preservation on the carbon isotope variations of dispersed organic matter in ancient floodplain sediments. Geochem. Geophys. Geosyst. 14, 4874–4891.

Blais, J.M., Kalff, J., 1995. The influence of lake morphometry on sediment focusing. Limnol. Oceanogr. 40, 582–588.

Bolle, M.P., Adatte, T., 2001. Palaeocene early Eocene climatic evolution in the Tethyan realm: clay mineral evidence. Clay Miner. 36, 249–261.

Bowen, G.J., Beerling, D.J., Koch, P.L., Zachos, J.C., Quattlebaum, T., 2004. A humid climate state during the Palaeocene/Eocene thermal maximum. Nature 432, 495–499.

Bowen, G.J., 2013. Up in smoke: a role for organic carbon feedbacks in Paleogene hyperthermals. Glob. Planet. Change 109, 18–29.

Bristow, T.F., Kennedy, M.J., Morrison, K.D., Mrofka, D.D., 2012. The influence of authigenic clay formation on the mineralogy and stable isotopic record of lacustrine carbonates. Geochim. Cosmochim. Acta 90, 64–82.

Charles, A.J., Condon, D.J., Harding, I.C., Pälike, H., Marshall, J.E.A., Cui, Y., Kump, L., Croudace, I.W., 2011. Constraints on the numerical age of the Paleocene–Eocene boundary. Geochem. Geophys. Geosyst. 12, Q0AA17. http://dx.doi.org/10.1029/2010GC003426.

Chikaraishi, Y., Naraoka, H., 2003. Compound-specific δD–δ^{13}C analyses of n-alkanes extracted from terrestrial and aquatic plants. Phytochemistry 63, 361–371.

Chung, F., 1974. Quantitative interpretation of X-ray diffraction patterns of mixtures. II. Adiabatic principle of X-ray diffraction analysis of mixtures. J. Appl. Crystallogr. 7, 526–531.

Clark, K.E., Hilton, R.G., West, A.J., Malhi, Y., Gröcke, D.R., Bryant, C.L., Ascough, P.L., Robles Caceres, A., New, M., 2013. New views on “old” carbon in the Amazon River: insight from the source of organic carbon eroded from the Peruvian Andes. Geochem. Geophys. Geosyst. 14, 1644–1659.

Clyde, W.C., Gingerich, P.D., 1998. Mammalian community response to the latest Paleocene thermal maximum: an isotaphonomic study in the northern Bighorn Basin, Wyoming. Geology 26, 1011–1014.

Cui, Y., Kump, L.R., Ridgwell, A.J., Charles, A.J., Junium, C.K., Diefendorf, A.F., Freeman, K.H., Urban, N.M., Harding, I.C., 2011. Slow release of fossil carbon during the Palaeocene–Eocene Thermal Maximum. Nat. Geosci. 4, 481–485.

DeConto, R.M., Galeotti, S., Pagani, M., Tracy, D., Schaefer, K., Zhang, T., Pollard, D., Beerling, D.J., 2012. Past extreme warming events linked to massive carbon release from thawing permafrost. Nature 484, 87–91.

Dickens, G.R., O’Neil, J.R., Rea, D.K., Owen, R.M., 1995. Dissociation of oceanic methane hydrate as a cause of the carbon isotope excursion at the end of the Paleocene. Paleoceanography 10, 965–971.

Dickson, J.A.D., Coleman, M.L., 1980. Changes in carbon and oxygen isotope composition during limestone diagenesis. Sedimentology 27, 107–118.

Feng, X., Epstein, S., 1995. Carbon isotopes of trees from arid environments and implications for reconstructing atmospheric CO_2 concentration. Geochim. Cosmochim. Acta 59, 2599–2608.

Feng, Z., Zhou, S., Wang, J., Gu, B., 1997. The changes of Meso-Cenozoic paleogeographic environments in the southwest of Henan. Henan Geol. 12, 270–277.

Feng, Z., Zhou, S., Li, Z., 1999. The age of the late cretaceous red beds in southwestern Henan Provence. Reg. Geol. China 3, 320–328.

Garzione, C.N., Dettman, D.L., Horton, B.K., 2004. Carbonate oxygen isotope paleoaltimetry: evaluating the effect of diagenesis on paleoelevation estimates for the Tibetan plateau. Palaeogeogr. Palaeoclimatol. Palaeoecol. 212, 119–140.

Giusberti, L., Rio, D., Agnini, C., Backman, J., Fornaciari, E., Tateo, F., Oddone, M., 2007. Mode and tempo of the Paleocene–Eocene thermal maximum in an expanded section from the Venetian pre-Alps. Geol. Soc. Am. Bull. 119, 391–412.

Gröcke, D.R., 1998. Carbon-isotope analyses of fossil plants as a chemostratigraphic and palaeoenvironmental tool. Lethaia 31, 1–13.

Handley, L., Pearson, P.N., McMillan, I.K., Pancost, R.D., 2008. Large terrestrial and marine carbon and hydrogen isotope excursions in a new Paleocene/Eocene boundary section from Tanzania. Earth Planet. Sci. Lett. 275, 17–25.

Hopmans, E.C., Weijers, J.W.H., Schefuss, E., Herfort, L., Sinninghe Damste, J.S., Schouten, S., 2004. A novel proxy for terrestrial organic matter in sediments based on branched and isoprenoid tetraether lipids. Earth Planet. Sci. Lett. 224, 107–116.

Huang, X., Li, C., Dawson, M.R., Liu, L., 2004. *Hanomys malcolmi*, a new simplicidentate mammal from the Paleocene of central China: its relationships and stratigraphic implications. Bull. Carnegie Mus. Nat. Hist. 36, 81–89.

John, C.M., Bohaty, S.M., Zachos, J.C., Sluijs, A., Gibbs, S., Brinkhuis, H., Bralower, T.J., 2008. North American continental margin records of the Paleocene–Eocene thermal maximum: implications for global carbon and hydrological cycling. Paleoceanography 23, PA2217. http://dx.doi.org/10.1029/2007PA001465.

Kennett, J.P., Stott, L.D., 1991. Abrupt deep-sea warming, palaeoceanographic changes and benthic extinctions at the end of the Palaeocene. Nature 353, 225–229.

Kent, D.V., Cramer, B.S., Lanci, L., Wang, D., Wright, J.D., der Voo, R.V., 2003. A case for a comet impact trigger for the Paleocene/Eocene thermal maximum and carbon isotope excursion. Earth Planet. Sci. Lett. 211, 13–26.

Koch, P.L., Zachos, J.C., Gingerich, P.D., 1992. Correlation between isotope records in marine and continental carbon reservoirs near the Paleocene/Eocene boundary. Nature 358, 319–322.

Kump, L.R., Arthur, M.A., 1999. Interpreting carbon-isotope excursions: carbonates and organic matter. Chem. Geol. 161, 181–198.

Kurtz, A.C., Kump, L.R., Arthur, M.A., Zachos, J.C., Paytan, A., 2003. Early Cenozoic decoupling of the global carbon and sulfur cycles. Paleoceanography 18, 1090. http://dx.doi.org/10.1029/2003PA000908.

Last, W.M., 1990. Lacustrine dolomite—an overview of modern, Holocene, and Pleistocene occurrences. Earth-Sci. Rev. 27, 221–263.

Leng, M.J., Marshall, J.D., 2004. Palaeoclimate interpretation of stable isotope data from lake sediments. Quat. Sci. Rev. 23, 811–831.

Leng, M.J., Jones, M.D., Frogley, M.R., Eastwood, W.J., Kendrick, C.P., Roberts, C.N., 2010. Detrital carbonate influences on bulk oxygen and carbon isotope composition of lacustrine sediments from the Mediterranean. Glob. Planet. Change 71, 175–182.

Ma, A., Cheng, J., 1991. On biostratigraphical subdivision of Yuhuangding formation in Liguanqiao Basin of eastern Qinling region. Sci. Geol. Sin. 1, 21–29.

Magioncalda, R., Dupuis, C., Smith, T., Steurbaut, E., Gingerich, P.D., 2004. Paleocene–Eocene carbon isotope excursion in organic carbon and pedogenic carbonate: direct comparison in a continental stratigraphic section. Geology 32, 553–556.

McCarren, H., Thomas, E., Hasegawa, T., Rohl, U., Zachos, J.C., 2008. Depth dependency of the Paleocene–Eocene carbon isotope excursion: paired benthic and terrestrial biomarker records (Ocean Drilling Program Leg 208, Walvis Ridge). Geochem. Geophys. Geosyst. 9, Q10008. http://dx.doi.org/10.1029/2008GC002116.

McInerney, F.A., Wing, S.L., 2011. The Paleocene–Eocene thermal maximum: a perturbation of carbon cycle, climate, and biosphere with implications for the future. Annu. Rev. Earth Planet. Sci. 39, 489–516.

Müller, G., Irion, G., Förstner, U., 1972. Formation and diagenesis of inorganic Ca–Mg carbonate in the lacustrine environment. Naturwissenschaften 59, 158–164.

Norris, R.D., Röhl, U., 1999. Carbon cycling and chronology of climate warming during the Palaeocene/Eocene transition. Nature 401, 775–778.

Pagani, M., Pedentchouk, N., Huber, M., Sluijs, A., Schoutern, S., Brinkhuis, H., Damsté, J.S.S., Dickens, G.R., et al., 2006a. Arctic hydrology during global warming at the Palaeocene/Eocene thermal maximum. Nature 442, 671–675.

Pagani, M., Caldeira, K., Archer, D., Zachos, J.C., 2006b. An ancient carbon mystery. Science 314, 1556–1557.

Panchuk, K., Ridgwell, A., Kump, L.R., 2008. Sedimentary response to Paleocene–Eocene Thermal Maximum carbon release: a model-data comparison. Geology 36, 315–318.

Poulson, S.R., John, B.E., 2003. Stable isotope and trace element geochemistry of the basal Bouse Formation carbonate, southwestern United States: implications for the Pliocene uplift history of the Colorado Plateau. Geol. Soc. Am. Bull. 115, 434–444.

Robert, C., Kennett, J.P., 1994. Antarctic subtropical humid episode at the Paleocene–Eocene boundary: clay-mineral evidence. Geology 22, 211–214.

Röhl, U., Westerhold, T., Bralower, T.J., Zachos, J.C., 2007. On the duration of the Paleocene–Eocene thermal maximum (PETM). Geochem. Geophys. Geosyst. 8, Q12002. http://dx.doi.org/10.1029/2007GC001784.

Schmidt, M.W.I., Noack, A.G., 2000. Black carbon in soils and sediments: analysis, distribution, implications, and current challenges. Glob. Biogeochem. Cycles 14, 777–793.

Schmitz, B., Pujalte, V., 2003. Sea-level, humidity, and land-erosion records across the initial Eocene thermal maximum from a continental–marine transect in northern Spain. Geology 31, 689–692.

Schneider-Mor, A., Bowen, G.J., 2013. Coupled and decoupled responses of continental and marine organic-sedimentary systems through the Paleocene–Eocene thermal maximum, New Jersey Margin, USA. Paleoceanography 28, 105–115.

Schoon, P.L., Heilmann-Clausen, C., Schultz, B.P., Sluijs, A., Damsté, J.S.S., Schouten, S., 2013. Recognition of Early Eocene global carbon isotope excursions using lipids of marine Thaumarchaeota. Earth Planet. Sci. Lett. 373, 160–168.

Schouten, S., Woltering, M., Rijpstra, W.I.C., Aluijs, A., Brinkhuis, H., Damsté, J.S.S., 2007. The Paleocene–Eocene carbon isotope excursion in higher plant organic matter: differential fractionation of angiosperms and conifers in the Arctic. Earth Planet. Sci. Lett. 258, 581–592.

Schubert, B.A., Hope Jahren, A., 2013. Reconciliation of marine and terrestrial carbon isotope excursions based on changing atmospheric CO_2 levels. Nat. Commun. 4, 1653.

Secord, R., Gingerich, P.D., Lohmann, K.C., Macleod, K.G., 2010. Continental warming preceding the Palaeocene–Eocene thermal maximum. Nature 467, 955–958.

Sluijs, A., Schouten, S., Pagani, M., Woltering, M., Brinkhuis, H., Damsté, J.S.S., Dickens, G.R., Huber, M., Reichart, G.J., Stein, R., Matthiessen, J., Lourens, L.J., Pedentchouk, N., Backman, J., Moran, K., et al., 2006. Subtropical arctic ocean temperatures during the Palaeocene/Eocene thermal maximum. Nature 441, 610–613.

Sluijs, A., Brinkhuis, H., Schouten, S., Bohaty, S.M., John, C.M., Zachos, J.C., Reichart, G.J., Damsté, J.S.S., Crouch, E.M., Dickens, G.R., 2007. Environmental precursors to rapid light carbon injection at the Palaeocene/Eocene boundary. Nature 450, 1218–1222.

Sluijs, A., Dickens, G.R., 2012. Assessing offsets between the δ^{13}C of sedimentary components and the global exogenic carbon pool across early Paleogene carbon cycle perturbations. Glob. Biogeochem. Cycles 26, GB4005. http://dx.doi.org/10.1029/2011GB004224.

Smith, F.A., Wing, S.L., Freeman, K.H., 2007. Magnitude of the carbon isotope excursion at the Paleocene–Eocene thermal maximum: the role of plant community change. Earth Planet. Sci. Lett. 262, 50–65.

Stoll, H.M., 2005. Limited range of interspecific vital effects in coccolith stable isotopic records during the Paleocene Eocene thermal maximum. Paleoceanography 20, PA1007. http://dx.doi.org/10.1029/2004PA001046.

Sun, Q., Chu, G., Liu, M., Xie, M., Li, S., Ling, Y., Wang, X., Shi, L., Jia, G., Lü, H., 2011. Distributions and temperature dependence of branched glycerol dialkyl glycerol tetraethers in recent lacustrine sediments from China and Nepal. J. Geophys. Res. 116, G01008. http://dx.doi.org/10.1029/2010JG001365.

Svensen, H., Planke, S., Malthe-Sorenssen, A., Jamtveit, B., Myklebust, R., Eidem, T.R., Rey, S.S., 2004. Release of methane from a volcanic basin as a mechanism for initial Eocene global warming. Nature 429, 542–545.

Tenzer, G.E., Meyers, P.A., Knoop, P., 1997. Sources and distribution of organic and carbonate carbon in surface sediments of Pyramid Lake, Nevada. J. Sediment. Res. 67, 884–890.

Thomas, D.J., Bralower, T.J., Zachos, J.C., 1999. New evidence for subtropical warming during the late Paleocene thermal maximum: stable isotopes from Deep Sea Drilling Project Site 527, Walvis Ridge. Paleoceanography 14, 561–570.

Thomas, D.J., Zachos, J.C., Bralower, T.J., Thomas, E., Bohaty, S., 2002. Warming the fuel for the fire: evidence for the thermal dissociation of methane hydrate during the Paleocene–Eocene thermal maximum. Geology 30, 1067–1070.

Thomas, E., 1998. The biogeography of the late Paleocene benthic foraminiferal extinction. In: Aubry, M.P., Lucas, S., Berggren, W.A. (Eds.), Late Paleocene–Early Eocene Biotic and Climatic Events in the Marine and Terrestrial Records. Columbia University Press, New York, pp. 214–243.

Ting, S.Y., Bowen, G.J., Koch, P.L., Clyde, W.C., Wang, Y., Wang, Y., McKenna, M.C., 2003. Biostratigraphic, chemostratigraphic, and magnetostratigraphic study across the Paleocene–Eocene boundary in the Hengyang Basin, Hunan, China. In: Wing, S.L., Gingerich, P.D., Schmitz, B., Thomas, E. (Eds.), Causes and Consequences of Globally Warm Climates in the Early Paleogene. Geological Society of America, Boulder, Colorado, pp. 521–535.

Tripati, A., Elderfield, H., 2005. Deep-sea temperature and circulation changes at the Paleocene–Eocene thermal maximum. Science 308, 1894–1898.

Weijers, J.W.H., Schouten, S., Sluijs, A., Brinkhuis, H., Damsté, J.S.S., 2007a. Warm arctic continents during the Palaeocene–Eocene thermal maximum. Earth Planet. Sci. Lett. 261, 230–238.

Weijers, J.W.H., Schouten, S., van den Donker, J.C., Hopmans, E.C., Sinninghe Damsté, J.S., 2007b. Environmental controls on bacterial tetraether membrane lipid distribution in soils. Geochim. Cosmochim. Acta 71, 703–713.

Wieczorek, R., Fantle, M.S., Kump, L.R., Ravizza, G., 2013. Geochemical evidence for volcanic activity prior to and enhanced terrestrial weathering during the Paleocene Eocene Thermal Maximum. Geochim. Cosmochim. Acta 119, 391–410.

Wing, S.L., Harrington, G.J., Smith, F.A., Bloch, J.I., Boyer, D.M., Freeman, K.H., 2005. Transient floral change and rapid global warming at the Paleocene–Eocene boundary. Science 310, 993–996.

Wright, J.D., Schaller, M.F., 2013. Evidence for a rapid release of carbon at the Paleocene–Eocene thermal maximum. Proc. Natl. Acad. Sci. USA 110, 15908–15913.

Zachos, J.C., Pagani, M., Sloan, L., Thomas, E., Billups, K., 2001. Trends, rhythms, and aberrations in global climate 65 Ma to present. Science 292, 686–693.

Zachos, J.C., Wara, M.W., Bohaty, S., Delaney, M.L., Petrizzo, M.R., Brill, A., Bralower, T.J., Premoli-Silva, I., 2003. A transient rise in tropical sea surface temperature during the Paleocene–Eocene Thermal Maximum. Science 302, 1551–1554.

Zachos, J.C., Röhl, U., Schellenberg, S.A., Sluijs, A., Hodell, D.A., Kelly, D.C., Thomas, E., Nicolo, M., Raffi, I., Lourens, L.J., McCarren, H., Kroon, D., 2005. Rapid acidification of the ocean during the Paleocene–Eocene thermal maximum. Science 308, 1611–1615.

Zachos, J.C., Schouten, S., Bohaty, S., Quattlebaum, T., Sluijs, A., Brinkhuis, H., Gibbs, S.J., Bralower, T.J., 2006. Extreme warming of mid-latitude coastal ocean during the Paleocene–Eocene Thermal Maximum: inferences from TEX86 and isotope data. Geology 34, 737–740.

Zachos, J.C., Dickens, G.R., Zeebe, R.E., 2008. An early Cenozoic perspective on greenhouse warming and carbon-cycle dynamics. Nature 451, 279–283.

Zeebe, R.E., Zachos, J.C., Dickens, G.R., 2009. Carbon dioxide forcing alone insufficient to explain Palaeocene–Eocene Thermal Maximum warming. Nat. Geosci. 2, 576–580.

Zhao, H., Guo, S., 1995. The Strata and Palaeontology of the Zhoukou and Nanyang in Henan Province. Geological Publishing House, Beijing.

Zhou, H., Hu, J., Ming, L., Peng, P., Zhang, G., 2011. Branched glycerol dialkyl glycerol tetraethers and paleoenvironmental reconstruction in Zoigê peat sediments during the last 150 years. Chin. Sci. Bull. 56, 2456–2463.

Zhu, M., Ding, Z., Wang, X., Chen, Z., Jiang, H., Dong, X., Ji, J., Tang, Z., Luo, P., 2010. High-resolution carbon isotope record for the Paleocene–Eocene thermal maximum from the Nanyang Basin, Central China. Chin. Sci. Bull. 55, 3606–3611.